AIMS Mathematics, 11(3): 8308–8331.
DOI: 10.3934/math.2026341
Received: 30 January 2026
Revised: 22 March 2026
Accepted: 24 March 2026
Published: 27 March 2026

https://www.aimspress.com/journal/Math

Research article

Reachable set estimation for wind energy conversion system via nonfragile memory sampled-data control

Raghul Venkateswaran[1], **Woosuk Choi**[1], **Jae Hoon Jeong**[2] **and Joo Woo**[2,*]

[1] Department of Artificial Intelligence and Data Science, Sejong University, 209, Neungdong-ro, Gwangjin-gu, Seoul 05006, Republic of Korea

[2] College of Computer and Software, Kunsan National University, 588 Daehak-ro, Gunsan-si, Jeonbuk 54150, Republic of Korea

* **Correspondence:** Email: oojoo1021@kunsan.ac.kr.

Abstract: This paper investigated the problem of reachable set estimation (RSE) and stabilization for nonlinear permanent magnet vernier generator (PMVG)-based wind energy conversion systems (WECSs) under external disturbances and control gain uncertainties. The inherent nonlinearity of the system, together with transmission delays and sampling effects, poses significant challenges for robust control design. To address these issues, a Takagi–Sugeno fuzzy modeling approach was employed to represent the nonlinear dynamics through a set of linear subsystems. A nonfragile memory-based sampled-data control (NFMSDC) scheme was developed to effectively address control gain perturbations, sampling constraints, and constant transmission delays. Stability conditions and RSE bounds were derived using Lyapunov–Krasovskii functionals and formulated as linear matrix inequalities, ensuring that system trajectories remain within prescribed ellipsoidal regions under bounded disturbances. The effectiveness of the proposed method was validated through numerical simulations, including wind disturbance scenarios and parameter variation analysis. The results show that the system states converge smoothly, the control inputs remain within practical limits, and the reachable sets are confined within the derived ellipsoidal bounds. Comparative analysis further demonstrated that the proposed approach achieves improved robustness and larger admissible sampling intervals compared to existing methods. These results confirm the practical applicability of the proposed NFMSDC scheme for PMVG-based WECSs under uncertain operating conditions.

Keywords: PMVG; eachable set estimation; T-S fuzzy control; memory sampled-data control; LMIs
Mathematics Subject Classification: 93C10, 93D05, 93D09, 93B52, 93C42

1. Introduction

In recent years, the wind power industry has increasingly turned its focus toward variable-speed wind turbine generators due to their significant advantages over traditional fixed-speed systems. These advantages include reduced noise emissions, higher power density, and enhanced control adaptability, which collectively improve energy efficiency and overall system performance [1, 2]. Variable-speed systems allow turbines to optimize their operation across a broader range of wind conditions, enabling them to capture more energy and respond dynamically to fluctuations in wind speed. Among these variable-speed technologies, direct-driven wind energy conversion systems (WECSs) utilizing permanent magnet vernier generator (PMVG) have gained particular attention. The gearless design of PMVG eliminates the need for mechanical gearboxes, resulting in lower mechanical complexity and reduced maintenance requirements [3]. This direct-drive configuration not only enhances system reliability but also improves operational efficiency, making PMVG an attractive solution for next-generation wind energy applications [4]. However, the integration of PMVG in WECS introduces unique challenges, particularly regarding system stability and performance under varying wind conditions.

Recent studies have explored these challenges, including a study that addressed maximizing power tracking in nonlinear PMVG-based WECS using a fuzzy control technique [5]. The rise of fuzzy-model (FM)-based control in industrial applications can be attributed to its effectiveness and simplicity in managing complex nonlinear systems [6]. The Takagi-Sugeno (T-S) FM (TSFM) is a widely utilized tool for designing and analyzing fuzzy control systems [7, 8]. Previous research has tackled the stability and stabilization issues of nonlinear chaotic systems, demonstrating that the T-S fuzzy technique effectively represents nonlinear models as linear sub-models through IF-THEN fuzzy membership functions [9, 10]. The T-S fuzzy technique has been popularly adopted in different real-world implementations, such as in helicopter and cancer-tumor immune systems [11, 12].

Advancements in digital technology have significantly increased the adoption of sampled-data control (SDC) systems, which offer distinct advantages over traditional continuous-time control methods [13–15]. SDC employs a digital computer to generate discrete-time control signals, which are then converted into continuous signals using a zero-order hold (ZOH) function [16]. For example, [17] addresses the stabilization problem for nonlinear systems through fuzzy SDC based on Lyapunov stability conditions. Similarly, [18] explores fuzzy SDC for nonlinear WECS, deriving stability conditions via the linear matrix inequalities (LMIs) approach. Furthermore, the authors in [19] demonstrated the effectiveness of the proposed H_∞ SDC for megawatt-class PMSG-based WECS, highlighting its practical efficacy.

In contrast, the memory SDC (MSDC) accounts for the constant transmission delay involved in signal transmission from the sampler to the controller and subsequently to the ZOH at time t_k, making it a more efficient option [20, 21]. The fuzzy membership-dependent Lyapunov–Krasovskii functionals (LKFs) proposed in [22] for permanent magnet synchronous machines established stability and stabilization conditions through MSDC. Furthermore, sufficient conditions for the stability and dissipativity of TSFM have been derived for permanent magnet synchronous motor (PMSM) systems using LKFs and relevant inequalities [23], while MSDC techniques have also been shown to ensure exponential stability in complex dynamical networks [24].

Despite these advancements, uncertainties in controller implementation remain a significant

challenge in industrial applications, often hindering the fulfillment of real-world requirements [25]. To address this issue, nonfragile control techniques have been developed to ensure robust controller performance even in the presence of uncertainties [26, 27]. For example, recent efforts such as finite-time synchronization and energy consumption prediction for multilayer fractional-order networks [28] and exponential synchronization approaches under Lévy noise and Markov switching [29] provide alternative frameworks for handling uncertainty and complex network dynamics, which are complementary to the nonfragile control design developed in this study. In addition, the authors in [24] explored the nonfragile MSDC (NFMSDC) framework for complex dynamical networks, while nonfragile control methods were also applied to the stabilization of chaotic systems and multi-agent systems in [30]. Recently, advanced disturbance rejection control strategies have been explored for networked systems. For instance, composite anti-disturbance control methods combined with event-triggered output feedback have been developed to address disturbances and actuator attacks, demonstrating improved robustness and resilience in practical control applications [31].

The topic of reachable set estimation (RSE) has recently attracted significant interest in the fields of robust control and practical applications [32, 33]. The RSE aims to enhance system safety by designing controllers that prevent the system from entering unsafe regions [34, 35]. This approach involves identifying regions where system states can reside, given zero initial conditions and bounded input disturbances [36, 37]. The RSE framework has been applied to large-scale nonlinear systems, with sufficient conditions obtained using LMIs [38]. Furthermore, the RSE problem for Markov jump systems has also been investigated [39]. Compared with existing works such as [23, 24, 34], the proposed non-fragile memory-based sampled-data control (NFMSDC) framework integrates reachable set estimation (RSE) with a sampled-data control strategy. While previous studies mainly investigate sampled-data control (SDC) or reachable set estimation separately, the proposed approach simultaneously considers RSE, transmission delays, sampling effects, and controller gain uncertainties within a unified framework for PMVG-based wind energy conversion systems. From a practical perspective, this integrated design improves system robustness against disturbances and uncertainties while ensuring that system states remain within a bounded safety region, which is essential for reliable operation of real-world wind energy systems. However, despite the progress made in RSE analysis, control uncertainties, and constant transmission delays for various nonlinear systems, there remains a lack of studies specifically addressing PMVG-based WECS, which serves as the main motivation for this study.

This study aims to investigate the design of RSE and NFMSDC for nonlinear PMVG-based WECS. The contributions of this study are summarized as follows:

1. This study develops a novel nonfragile memory-based sampled-data controller scheme for a 5-kW permanent magnet vernier generator-based wind energy conversion system with nonlinear boost converters. The controller effectively handles parameter uncertainties and sampling effects, thereby ensuring improved control performance and stability.
2. A delay-dependent LKF framework is formulated to establish sufficient conditions for reachable set estimation and exponential stabilization. This approach offers tighter safety bounds, enhancing the reliability of wind energy conversion system operation under fluctuating wind conditions.
3. Extensive numerical simulations and two detailed case studies, along with comparative analyses against existing approaches [23], verify that the proposed nonfragile memory-based sampled-data controller achieves a larger admissible sampling bound, stronger robustness, and practical

feasibility for real-world wind energy applications.

The remainder of this paper is organized as follows. Section 2 presents the modeling of the PMVG-based WECS and its T-S fuzzy representation. Section 3 develops the RSE and stabilization conditions based on LKFs. Section 4 provides numerical simulations to verify the effectiveness of the proposed NFMSDC scheme. Finally, Section 5 concludes the paper.

Notations: In this paper, $\mathbb{R}^n$ denotes the Euclidean n-dimensional space. To indicate the positive (negative) definite of a real symmetric matrix, we write it as $\mathcal{R} > (<)\ 0$. Matrix inverses and transposes are indicated by the superscripts -1 and T. Here, $diag\{\cdots\}$ and $Sym\{\mathcal{R}\}$ stand for the diagonal matrix and $\mathcal{R} + \mathcal{R}^T$, respectively. The symbol $*$ is used to indicate symmetry in a matrix.

2. Modeling of the PMVG-based WECS

This section presents a non-linear model of the PMVG-based WECS and its corresponding TSFM as displayed in Figure 1.

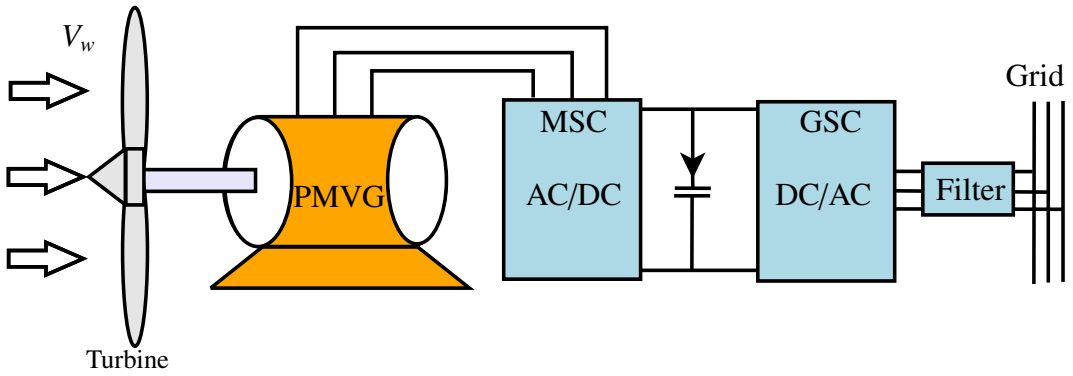

Figure 1. Schematic representation of the PMVG-based WECS diagram.

2.1. PMVG-based WECS

The total amount of energy $P_{turbine}$ captured by the wind turbine can be expressed as follows [4]:

$$P_{turbine} = 0.5C_p(\lambda,\beta)\rho\pi R^2 V_w^3, \tag{2.1}$$

where ρ is air density, R represents the blade length, V_w is the wind speed, the WECS power coefficient C_p, which is a function of λ and pitch angle β is stated as follows [4]:

$$C_p(\lambda,\beta) = 0.73\left(\frac{151}{\lambda_i} - 0.58\beta - 0.002\beta^{2.14} - 13.2\right)e^{\left(\frac{-18.4}{\lambda_i}\right)}. \tag{2.2}$$

The tip speed ratio λ can be written as follows [4]:

$$\lambda = \frac{r\omega_t}{V_w}, \tag{2.3}$$

where ω_t is the speed of the turbine.

2.2. Modeling of the PMVG

In this subsection, the dynamical model of the PMVG can be expressed as [4]

$$\begin{cases} V_{sd} & = R_s I_{sd}(t) - W_m L_d L_q + L_d \frac{dI_{sd}(t)}{dt} \\ V_{sq} & = R_s I_{sq}(t) + W_m L_d L_q + L_q \frac{dI_{sq}(t)}{dt} + W_m \Psi_{mag} \\ T_e & = 1.5 n_p I_{sq}(t) \Psi_{mag} \\ \frac{dW_m(t)}{dt} & = \frac{1}{J}(C_t - T_e - f_c W_m(t)). \end{cases} \tag{2.4}$$

The above set of equations represents the dynamic model of the PMVG in the dq-reference frame. Here, I_{sd} and I_{sq} denote the d- and q-axis stator currents, while V_{sd} and V_{sq} represent the corresponding stator voltages. The parameters L_d and L_q are the d- and q-axis inductances, respectively, and R_s is the stator resistance. The term W_m indicates the electrical angular speed of the rotor, and Ψ_{mag} refers to the permanent magnet flux linkage. The electromagnetic torque T_e is expressed as a function of the q-axis current and flux linkage, where n_p represents the number of pole pairs. The mechanical dynamics are governed by the rotor inertia J, viscous friction coefficient f_c, and the applied mechanical (shaft) torque C_t, which together determine the rotor speed variation $\frac{dW_m}{dt}$. Continually, the shaft torque C_t can be described as follows [4]:

$$C_t = \frac{1}{2}\rho\pi R^3 \frac{C_p(\lambda,\beta)}{\lambda} V_w^2. \tag{2.5}$$

Based on the (2.1)–(2.5), the overall nonlinear dynamic representation of the PMVG-based WECS can be expressed in the state-space representation as follows [4]:

$$\dot{x}(t) = A(x)x(t) + Bu(t) + Dw(t), \tag{2.6}$$

where $x(t) = [W_m(t)\ I_{sq}(t)\ I_{sd}(t)]^T$ denotes the state vector; $u = [V_{sq}\ V_{sd}]^T$ represents the control input; D denotes the external disturbance matrix. Then, we assume the peak disturbance input bound can be satisfied by the following the condition:

$$w^T(t)w(t) \le \bar{w}^2, \quad t \ge 0, \tag{2.7}$$

where $\bar{w}$ denotes the positive scalars.

$$A(x) = \begin{bmatrix} -\frac{(f_c + C_{tt}W_m(t))}{J} & \frac{1.5\Psi_{\text{mag}}}{J} & 0 \\ -\frac{\Psi_{mag}}{L_q} & -\frac{R_s}{L_q} & -\frac{L_d W_m(t)}{L_q} \\ 0 & \frac{L_q W_m(t)}{L_d} & -\frac{R_s}{L_d} \end{bmatrix},$$

$$B = \begin{bmatrix} 0 & 0 \\ -\frac{1}{L_q} & 0 \\ 0 & \frac{1}{L_d} \end{bmatrix},\ C_{tt} = \frac{0.5\rho\pi R^5 C_{pmax}}{\lambda^3}, W_m(t) \in [d_1,\ d_2].$$

2.2.1. Wind disturbance characterization

The external disturbance $w(t) = V_w$ represents wind-induced aerodynamic fluctuations that act on the mechanical state $W_m(t)$ of the PMVG system. Due to atmospheric inertia, wind exhibits cumulative energy effects that are modeled as

$$w(t) = \sigma \left| \int_0^t \xi(\tau)\, d\tau \right|, \tag{2.8}$$

where $\xi(\tau)$ is a white-noise process representing instantaneous wind turbulence, and $\sigma = 0.0001$ is an intensity scaling parameter that determines the magnitude of the disturbance. The absolute value ensures a non-negative disturbance magnitude consistent with aerodynamic torque characteristics in WECS. This disturbance formulation captures the stochastic and persistent nature of wind fluctuations while still satisfying the bounded disturbance condition given in (2.7). Consequently, the disturbance model provides a realistic representation of atmospheric turbulence and enables evaluation of the robustness of the proposed controller under fluctuating wind conditions.

2.3. T-S fuzzy modelling of the PMVG-based WECS

In this subsection, the nonlinear system (2.6) and its associated T-S fuzzy system (TSFS) are explained. The Eq (2.6) includes a nonlinear component that arises from the multiplication involving $W_m(t)$, which introduces nonlinear coupling into the system dynamics. By constructing a set of fuzzy rules with corresponding membership functions, the nonlinear system can be approximated by several local linear models. This representation significantly simplifies controller design because stability conditions can be derived using linear matrix inequalities while preserving the essential nonlinear characteristics of the PMVG system. Since stabilizing such a nonlinear model is inherently more challenging, the nonlinear dynamics of the PMVG-based WECS are reformulated into an equivalent structure using a type-1 fuzzy modeling approach:

$$\dot{x}(t) = \sum_{i=1}^{2} \varphi_i(x_1(t)) \left\{ \mathcal{A}_i x(t) + B_i u(t) + D_i w(t) \right\}, \tag{2.9}$$

where

$$A_1 = \begin{bmatrix} -\frac{(f_c + C_{tt} d_1)}{J} & \frac{1.5\Psi_{\text{mag}}}{J} & 0 \\ -\frac{\Psi_{mag}}{L_q} & -\frac{R_s}{L_q} & -\frac{L_d d_1}{L_q} \\ 0 & \frac{L_q d_1}{L_d} & -\frac{R_s}{L_d} \end{bmatrix}, \; A_2 = \begin{bmatrix} -\frac{(f_c + C_{tt} d_2)}{J} & \frac{1.5\Psi_{\text{mag}}}{J} & 0 \\ -\frac{\Psi_{mag}}{L_q} & -\frac{R_s}{L_q} & -\frac{L_d d_2}{L_q} \\ 0 & \frac{L_q d_2}{L_d} & -\frac{R_s}{L_d} \end{bmatrix},$$

$$B_1 = B_2 = \begin{bmatrix} 0 & 0 \\ -\frac{1}{L_q} & 0 \\ 0 & \frac{1}{L_d} \end{bmatrix}, D_1 = D_2 = [1\ 0\ 0]^T.$$

Then, the corresponding membership functions are $\varphi_1(x_1(t)) = \frac{d_2 - W_m(t)}{d_2 - d_1}$ and $\varphi_2(x_1(t)) = 1 - \varphi_1(x_1(t))$.

2.4. Design of the nonfragile fuzzy memory-based sampled-data controller

In this subsidiary section, the design of nonfragile NFMSDC for PMVG-based WECS is discussed. Then, the overall schematic representation is displayed in Figure 2. In order to design the NFMSDC, we assume that the control signal appears through ZOH with a sequence of hold times $0 = t_0 < t_1 < \cdots < t_k < \cdots \lim_{k\to\infty} t_k = \infty$. Based on this, the corresponding NFMSDC is defined as follows:

Controller rule j: IF $\upsilon_1(t_k)$ is $\Re_{j1}$ and $\upsilon_2(t_k)$ is $\Re_{j2}$, THEN

$$u(t) = (\mathcal{M}_j + \Delta\mathcal{M}_j(t))x(t - h(t)) + (\mathcal{N}_j + \Delta\mathcal{N}_j(t)) \times x(t - h(t) - \sigma),\ t \in [t_k, t_{k+1}),\ j = 1, 2, 3, 4 \tag{2.10}$$

where $\mathcal{M}_j$ and $\mathcal{N}_j$ are the gain matrices, σ represents the memory parameter, $h(t) = t - t_k$ is a piecewise linear function statifies $0 < t_{k+1} - t_k = h_k \leq h$, and h denotes the maximum sampling interval (MSI). The possible variations in controller gains are represented by the uncertainties $\Delta\mathcal{M}_j(t)$ and $\Delta\mathcal{N}_j(t)$. The $\Delta\mathcal{M}_j(t)$ and $\Delta\mathcal{N}_j(t)$ are considered as having the following form:

$$[\Delta\mathcal{M}_j(t) \quad \Delta\mathcal{N}_j(t)] = Q_j R_j(t)[S_j \quad T_j],$$

where Q_j, S_j, and T_j are the known constant matrices, and $R_j(t)$ is an unknown matrix satisfying $R_j^T(t)R_j(t) \leq I$. Therefore, the overall form of the NFMSDC is as follows:

$$u(t) = \sum_{j=1}^{2} \varphi_j(x_1(t_k))(\mathcal{M}_j + \Delta\mathcal{M}_j(t))x(t - h(t)) + (\mathcal{N}_j + \Delta\mathcal{N}_j(t)) \times x(t - h(t) - \sigma),\ t \in [t_k, t_{k+1}). \tag{2.11}$$

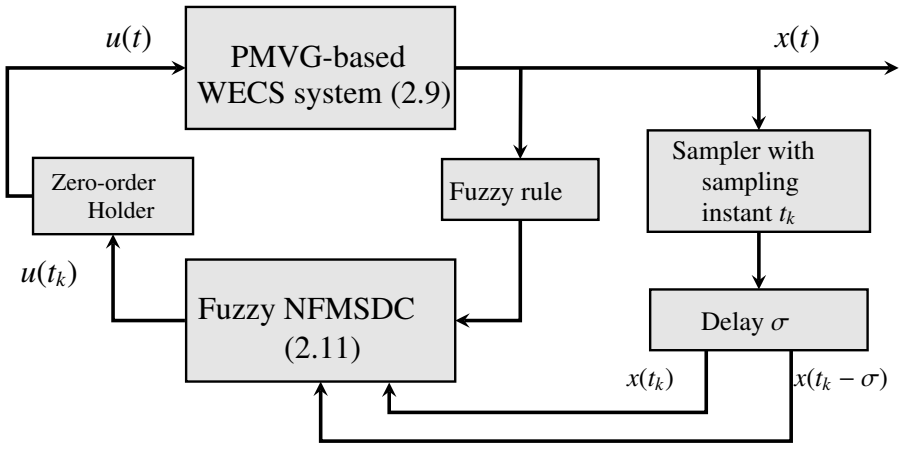

Figure 2. Schematic representation of the proposed NFMSDC with fuzzy approach.

Substituting NFMSDC (2.11) into (2.9), the closed-loop PMVG-based WECS can be defined in the following form:

$$\dot{x}(t) = \sum_{i=1}^{2}\sum_{j=1}^{2} \varphi_i(x_1(t))\varphi_j(x_1(t_k))\{\mathcal{A}_i x(t) + B_i\{(\mathcal{M}_j + \Delta\mathcal{M}_j(t))x(t - h(t))$$

$$+ (\mathcal{N}_j + \Delta\mathcal{N}_j(t))x(t - h(t) - \sigma)\} + D_i w(t)\}. \tag{2.12}$$

Next, we discuss RSE for the considered nonlinear PMVG system (2.6), where all the system states are bounded by

$$\mathcal{S} \triangleq \{x(t) \in \mathbb{R}^n | x(t), w(t) \text{ satisfy } (2.6), (2.7), t \geq 0\}. \tag{2.13}$$

The method presented in [33] provides a framework for determining the RSE of the closed-loop system (2.12) by constructing an ellipsoid that bounds the RSE. Determination of the ellipsoid is based on a positive definite matrix $\mathcal{Z}$, which serves to guarantee the system's robustness against uncertainties and disturbances. The results of [33] provide a basis for the design of controllers that ensure safe operation of the PMVG-based WECS (2.12).

$$\epsilon \triangleq \{x \in \mathcal{Z}^n | x^T \mathcal{Z} x \leq 1\}. \tag{2.14}$$

Lemma 1. *[33] Given the closed-loop PMVG-based WECS* (2.12) *and any ellipsoidal bound* $\mathcal{E}(0, \mathcal{Z})$ *of its RSE, there exists a constant* $K > 0$ *such that*

$$|x(t)| \leq \mathcal{K} |x(0)|, \tag{2.15}$$

for all $x(0) \in \mathcal{E}(0, \mathcal{Z})$ *and* $t \geq 0$.

Lemma 2. *[33] For the considered system* (2.12)*, let* $V(t)$ *be a Lyapunov function, where* $\alpha > 0$*. If* $\dot{V}(t) + \alpha V(t) - \frac{\alpha}{\bar{w}} w^T(t) w(t) \leq 0$*, then* $V(x(t)) \leq 1$.

Lemma 3. *[16] For a continuous differentiable function* $x : [c,\ d] \to \mathbb{R}^n$*, a given symmetric matrix* $\mathcal{S} > 0,\ W_1 \in \mathbb{R}^{n \times n}$*, and* $W_2 \in \mathbb{R}^{n \times n}$*, the following inequality holds*

$$-\int_c^d \dot{x}^T(t) \mathcal{S} \dot{x}(t) ds \leq \psi^T(c, d) \Theta \psi(c, d), \tag{2.16}$$

where $c < d$,

$$\begin{aligned} \Theta &= (d - c)(W_1 S^{-1} W_1^T + \frac{(d - c)^2}{3} W_2 S^{-1} W_2^T \\ &\quad - Sym\{W_2\ W_2\ 0\}) + Sym\{[W_1\ -W_1 2 W_2]\}, \\ \psi(c, d) &= \left[x^T(d), x^T(c), \int_c^d x^T(s) ds \right]^T. \end{aligned}$$

The above lemmas serve as the foundation for the main results and prove the feasibility of the designed RSE and NFMSDC design for considered system (2.12).

Problem 1. *The objectives of this paper are to design and validate a solution for the RSE problem for PMVG-based WECS* (2.12) *using the NFMSDC approach.*

- *The boundedness of the RSE with input constraint* (2.7) *in PMVG-based WECS* (2.12) *is confirmed through the use of LMIs, which are derived in the form of delay-dependent sufficient criteria and satisfy the ellipsoid condition stated in* (2.14)*.*
- *The appropriate control gain matrices* $\mathcal{M}_j$ *and* $\mathcal{N}_j$ *are calculated by solving LMIs.*

3. Main results

In this section, Theorem 1 achieves the RSE and stability analysis of the PMVG-based WECS (2.12), and Theorem 2 provides the RSE and stabilization analysis of the considered system.

3.1. Stability analysis

Theorem 1. *For known scalars $h_k \in (0, h]$, $\alpha > 0$, $\gamma > 0$, $\beta > 0$, $\bar{w} > 0$, and matrices $\varpi > 0$, the constant time-delay $\sigma > 0$, the control gains are $\mathcal{M}_j$ and $\mathcal{N}_j$, the RSE of PMVG-based WECS* (2.12) *is bounded in $\epsilon(\varpi, 1)$, if there exists positive symmetric matrices $\mathcal{Z}, \mathcal{Z}_1, \mathcal{X}_{11}, \mathcal{X}_{14}, \mathcal{X}_{16}, \mathcal{P}_1, \mathcal{P}_3, T_1, \mathcal{Z}_2$, any matrices $\mathcal{X}_{12}, \mathcal{X}_{13}\, \mathcal{X}_{15}, \mathcal{P}_2, \bar{\mathcal{G}}_1, \bar{\mathcal{G}}_2, \bar{\mathcal{G}}_3$, W_{1l}, W_{2l} $(l = 1, 2, 3, 4, 5, 6, 7)$, satisfying the following LMIs:*

$$\begin{bmatrix} -\mathcal{Z} & I \\ * & -\varpi^{-1} \end{bmatrix} \leq 0, \tag{3.1}$$

$$\begin{bmatrix} \Theta^{ij}_{(h_k,0)} & \Xi_1 & \frac{h^2}{4}\Xi_2 \\ * & -\varepsilon I_n & 0 \\ * & * & -\frac{h^2}{4}\mathcal{O} \end{bmatrix} < 0, \tag{3.2}$$

$$\begin{bmatrix} \Theta^{ij}_{(h_k,h_k)} + h\Xi_3 & W_{1l} & W_{2l} & \Xi_1 & \frac{h^2}{4}\Xi_2 \\ * & -h\mathcal{P}_1 & 0 & 0 & 0 \\ * & * & -\frac{h^3}{3}\mathcal{P}_1 & 0 & 0 \\ * & * & * & -\varepsilon I_n & 0 \\ * & * & * & * & -\frac{h^2}{4}\mathcal{O} \end{bmatrix} < 0, \tag{3.3}$$

where $\Theta^{ij}_{(h_k,h(t))}$ can be stated as

$$\begin{aligned}
&\Theta^{ij}_{(h_k,h(t))} = \\
&Sym\{\mathrm{e}_1^T\mathcal{Z}\mathrm{e}_5 + \frac{\pi^2}{4}e^{-\alpha\sigma}\mathrm{e}_3\mathcal{Z}_2\mathrm{e}_4 - h(t)(\mathrm{e}_1^T\mathcal{X}_{12}\mathrm{e}_2 + \mathrm{e}_1^T\mathcal{X}_{13}\mathrm{e}_3 + \mathrm{e}_2^T\mathcal{X}_{15}\mathrm{e}_3)(h_k - h(t))(\mathrm{e}_1^T\mathcal{Z}_1\mathrm{e}_5 \\
&- \mathrm{e}_2^T\mathcal{Z}_1\mathrm{e}_5 + \alpha\mathrm{e}_1^T\mathcal{Z}_1\mathrm{e}_2 + \mathrm{e}_1^T\mathcal{X}_{12}\mathrm{e}_2 + \mathrm{e}_1^T\mathcal{X}_{13}\mathrm{e}_3 + \mathrm{e}_2^T\mathcal{X}_{15}\mathrm{e}_3 + \mathrm{e}_2^T\mathcal{P}_2^T\mathrm{e}_5)\} + \Xi_4 + \alpha\mathrm{e}_1^T\mathcal{Z}\mathrm{e}_1 \\
&- h(t)(\mathrm{e}_1^T\mathcal{X}_{11}\mathrm{e}_1 + \mathrm{e}_2^T e^{\alpha h}h(t)\mathcal{P}_3\mathrm{e}_2 + \mathrm{e}_2^T\mathcal{X}_{14}\mathrm{e}_2 + \mathrm{e}_3^T\mathcal{X}_{16}\mathrm{e}_3) + (h_k - h(t))(\alpha\mathrm{e}_1^T\mathcal{Z}_1\mathrm{e}_1 \\
&- \alpha\mathrm{e}_2^T\mathcal{Z}_1\mathrm{e}_2 + \mathrm{e}_1^T\mathcal{X}_{11}\mathrm{e}_1 + \mathrm{e}_2^T\mathcal{X}_{14}\mathrm{e}_2 + \mathrm{e}_3^T\mathcal{X}_{16}\mathrm{e}_3 + \mathrm{e}_5^T\mathcal{P}_1\mathrm{e}_5 - \mathrm{e}_2^T\mathcal{P}_3\mathrm{e}_2) + \mathrm{e}_5^T\frac{h^2}{4}\mathcal{O}\mathrm{e}_5 - \mathrm{e}_1^T e^{\alpha h}\mathcal{P}_2\mathrm{e}_2 \\
&+ \mathrm{e}_2^T 2e^{\alpha h}\mathcal{P}_2\mathrm{e}_2 + \mathrm{e}_1^T\sigma\mathcal{T}_1\mathrm{e}_1 - \mathrm{e}_4^T\sigma e^{-\alpha\sigma}\mathcal{T}_1\mathrm{e}_4 + \mathrm{e}_5\mathcal{Z}_2\mathrm{e}_5 - \frac{\pi^2}{4}e^{-\alpha\sigma}(\mathrm{e}_3\mathcal{Z}_2\mathrm{e}_3 + \mathrm{e}_4\mathcal{Z}_2\mathrm{e}_4) \\
&+ Sym\{\mathrm{e}_1^T\bar{\mathcal{G}}_1^T + \mathrm{e}_3^T\bar{\mathcal{G}}_2^T + \mathrm{e}_5^T\bar{\mathcal{G}}_3^T\}[-\mathrm{e}_5 + \mathcal{A}_i\mathrm{e}_1 + B_i\mathcal{M}_j\mathrm{e}_2 + B_i\mathcal{N}_j\mathrm{e}_3 \\
&+ D_i\mathrm{e}_7] + \varepsilon\Xi_5 B_i Q_j Q_j^T B_i^T\Xi_5^T,
\end{aligned}$$

$$\Xi_1 = (S_j\mathrm{e}_2^T + T_j\mathrm{e}_3^T)diag\{\mathcal{G}\,\mathcal{G}\,\mathcal{G}\,\mathcal{G}\,\mathcal{G}\,\mathcal{G}\,\mathcal{G}\}, \ \Xi_2 = [\mathcal{X}_{11}\,\mathcal{X}_{12}\,\mathcal{X}_{13}\,0\,0\,0\,0]^T,$$

$$\Xi_3 = Sym\{[W_{2l}\,W_{2l}\,0\,0\,0\,0\,0]\}, \Xi_4 = Sym\{[W_{1l}\ -W_{1l}\,0\,0\,0\,2W_{2l}\,0]\},$$

$$\Xi_5 = \mathrm{e}_1 M_1^T + \mathrm{e}_3 M_2^T + \mathrm{e}_5 M_3^T,$$

$$\mathcal{X} = \begin{bmatrix} \mathcal{X}_{11} & \mathcal{X}_{12} & \mathcal{X}_{13} \\ * & \mathcal{X}_{14} & \mathcal{X}_{15} \\ * & * & \mathcal{X}_{16} \end{bmatrix}, \ \mathcal{P} = \begin{bmatrix} \mathcal{P}_1 & \mathcal{P}_2 \\ * & \mathcal{P}_3 \end{bmatrix}.$$

The LKF is constructed to capture the dynamic characteristics of the PMVG-based WECS under sampled-data control and time-delay effects. The term $V_1(t)$ represents the instantaneous energy of the system states. The terms $V_2(t)$ and $V_3(t)$ characterize the sampling interval dynamics and delay-dependent behavior between sampling instants. The component $V_4(t)$ captures the influence of the constant transmission delay, while $V_5(t)$ reflects the energy associated with the derivative of the system states. This structured construction enables the derivation of delay-dependent stability conditions and reachable set estimation bounds.

Proof. Construct the LKF for considered PMVG-based WECS (2.12)*:*

$$V(t) = \sum\nolimits_{m=1}^{5} V_m(t),$$

where

$$V_1(t) = x^T(t)\mathcal{Z}x(t),\ V_2(t) = (t_{k+1}-t)(t-t_k)\mathcal{J}_1^T\mathcal{X}\mathcal{J}_1,$$
$$V_3(t) = (t_{k+1}-t)\int_{t_k}^{t} e^{\alpha(s-t)}\mathcal{J}_2^T\mathcal{P}\mathcal{J}_2 ds + (t_{k+1}-t)\mathcal{J}_3^T\mathcal{Z}_1\mathcal{J}_3,$$
$$V_4(t) = \sigma\int_{t-\sigma}^{t} e^{\alpha(s-t)}x^T(s)\mathcal{T}_1 x(s)ds,$$
$$V_5(t) = h^2\int_{t_k-\sigma}^{t} e^{\alpha(s-t)}\dot{x}^T(t)\mathcal{Z}_2\dot{x}(t)ds - \frac{\pi^2}{4}\int_{t_k-\sigma}^{t-\sigma} e^{\alpha(s-t)}\mathcal{J}_4^T\mathcal{Z}_2\mathcal{J}_4 ds,$$

with

$$\mathcal{J}_1 = \begin{bmatrix} x(t) \\ x(t_k) \\ x(t_k-\sigma) \end{bmatrix}, \quad \mathcal{J}_2 = \begin{bmatrix} \dot{x}(s) \\ x(t_k) \end{bmatrix},$$
$$\mathcal{J}_3 = (x(t)-x(t_k)), \quad \mathcal{J}_4 = (x(s)-x(t_k-\sigma)),$$

where $\dot{V}(t)$ are calculated as

$$\dot{V}_1(t) = -\alpha V_1(t) + 2x^T(t)\mathcal{Z}\dot{x}(t) + x^T(t)\alpha\mathcal{Z}x(t), \tag{3.4}$$
$$\dot{V}_2(t) = -\alpha V_2(t) - (t-t_k)\mathcal{J}_1^T\mathcal{X}\mathcal{J}_1 + (t_{k+1}-t)\mathcal{J}_1^T\mathcal{X}\mathcal{J}_1 + 2(t_{k+1}-t)(t-t_k)\xi^T(t)\Xi_2\dot{x}(t), \tag{3.5}$$
$$\dot{V}_3(t) = -\alpha V_3(t) - \int_{t_k}^{t} e^{\alpha(s-t)}\mathcal{J}_2^T\mathcal{P}\mathcal{J}_2 + (t_{k+1}-t)\begin{bmatrix} \dot{x}(t) \\ x(t_k) \end{bmatrix}^T\mathcal{P}\begin{bmatrix} \dot{x}(t) \\ x(t_k) \end{bmatrix} - \mathcal{J}_3^T\mathcal{Z}_1\mathcal{J}_3 + 2(t_{k+1}-t)\mathcal{J}_3^T\mathcal{Z}_1\dot{x}(t) + (t_{k+1}-t)\mathcal{J}_3^T\alpha\mathcal{Z}_1\mathcal{J}_3. \tag{3.6}$$

Applying the Lemma 3, we have

$$-\int_{t_k}^{t}\dot{x}^T(s)\mathcal{P}_1\dot{x}(s)ds \le \xi^T(t)\Theta\xi(t), \tag{3.7}$$

where

$$\Theta = (t-t_k)[W_{1l}\mathcal{P}_1^{-1}W_{1l}^T + \frac{h^2}{3}W_{2l}\mathcal{P}_1^{-1}W_{2l}^T + \Xi_3] + \Xi_4$$

$$\dot{V}_4(t) = -\alpha V_4(t) + x^T(t)\sigma\mathcal{T}_1 x(t) - x^T(t-\sigma)\sigma e^{-\alpha\sigma}\mathcal{T}_1 x^T(t-\sigma), \tag{3.8}$$

$$\dot{V}_5(t) = -\alpha V_5(t) + \dot{x}^T(t)\mathcal{Z}_2\dot{x}(t) - \frac{\pi^2}{4}e^{-\alpha\sigma}(x(t-\sigma) - x(t_k-\sigma))^T\mathcal{Z}_2(x(t-\sigma) - x(t_k-\sigma)). \tag{3.9}$$

From $\dot{V}_2(t)$ *and any positive definite matrix* $\mathcal{O} \in \mathbb{R}^{n\times n}$, *the following inequality holds*

$$2(t_{k+1}-t)(t-t_k)\xi^T(t)\Xi_2\dot{x}(t) \le \frac{h^2}{4}(\xi^T(t)\Xi_2\mathcal{O}^{-1}\Xi_2^T\xi(t) + \dot{x}^T(t)\mathcal{O}\dot{x}(t)).$$

From (2.12), *it is easy to obtain that the appropriate dimension matrices* $\bar{\mathcal{G}}_1^T, \bar{\mathcal{G}}_2^T$, *and* $\bar{\mathcal{G}}_3^T$:

$$0 = 2\zeta(t)\sum_{i=1}^{4}\sum_{j=1}^{4}\varphi_i(\upsilon(t))\varphi_j(\upsilon(t_k))(\mathcal{A}_i x(t) + B_i\{(\mathcal{M}_j + \Delta\mathcal{M}_j(t))x(t-h(t)) + (\mathcal{N}_j + \Delta\mathcal{N}_j(t))x(t-h(t)-\sigma)\}, \tag{3.10}$$

where $\zeta(t) = x^T(t)\bar{\mathcal{G}}_1^T + x^T(t_k-\sigma)\bar{\mathcal{G}}_2^T + \dot{x}^T(t)\bar{\mathcal{G}}_3^T$. *Applying Lemma [14] for a given scalar* $\varepsilon > 0$, *one can obtain*

$$\begin{aligned}&2\zeta(t)B_i[\Delta\mathcal{M}_j(t)x(t-h(t)) + \Delta\mathcal{N}_j(t)x(t-h(t)-\sigma)]\\ &\le\varepsilon\zeta(t)B_iQ_jQ_j^TB_i^T\zeta^T(t) + \varepsilon^{-1}[S_j x(t-h(t)) + T_j x(t-h(t)-\sigma)]^T[S_j x(t-h(t)) + T_j x(t-h(t)-\sigma)].\end{aligned} \tag{3.11}$$

Consolidating from (3.4)–(3.11), *it obtain that*

$$\dot{V}(t) + \alpha V(t) - \frac{\alpha}{w^2}w^T(t)w(t) \le \sum_{i=1}^{4}\sum_{j=1}^{4}\varphi_i(\upsilon(t))\varphi_j(\upsilon(t_k)) \times \xi^T(t)\left[\frac{h_k - h(t)}{h_k}\Theta_{(h_k,0)}^{ij} + \frac{h(t)}{h_k}\Theta_{(h_k,h_k)}^{ij}\right]\xi(t), \tag{3.12}$$

where

$$\xi^T(t) = [x^T(t)\ x^T(t_k)\ x^T(t_k-\sigma)\ x^T(t-\sigma)\dot{x}(t)\int_{t_k}^{t}x^T(s)ds\ w^T(t)].$$

From (3.12), *we know that the convex combination of* $\Theta_{(h_k,0)}^{ij}$ *and* $\Theta_{(h_k,h_k)}^{ij}$ *is* $\Theta_{(h_k,h(t))}^{ij}$. *Also,* $\Theta_{(h_k,h(t))}^{ij} < 0$ *if and only if* (3.2) *and* (3.3) *hold. Since* $lim_{t-t_k}\ V_2(t) = V_2(t_k) = 0$ *and* $lim_{t-t_k}\ V_3(t) = V_3(t_k) = 0$, *we note that* $\{\mathcal{X}, \mathcal{P}, \mathcal{Z}_1\}-$*dependent terms* $V_2(t)$ *and* $V_3(t)$ *disappear at the sampling instant* t_k. *Then* $V_4(t)+V_5(t) \ge 0$ *implies that* $V_1(t) \le 1$. *It is easy to see that* V_1 *is the intersection of the ellipsoid. Based on Lemmas 1 and 2, the RSE of the PMVG-based WECS* (2.12) *is bounded by* $\epsilon = \{x \in \mathcal{Z}^n | x^T\mathcal{Z}x \le 1\}$. *Meanwhile, one can obtain* $0 < \varpi \le \mathcal{Z}$. *Consequently, it can be inferred that* $\epsilon\{x^T\varpi x\} \le \epsilon\{x^T\mathcal{Z}x\}$. *Hence, the proof is complete.* □

Remark 1. *In recent years, the main objective of the reachable set estimation for the TSFS is to acquire the ellipsoid $\epsilon(\mathcal{Z})$, which needs to be minimized for a prescribed constant α. To address this, an additional inequality* (3.1) *is presented in Theorem 1, defining the matrix ϖ as $\varpi = \theta_{max}I$ and subsequently maximizing a constant θ_{max}.*

Remark 2. *Theorem 1 refers to the fact that the condition for stability of the system described in Eq* (2.12) *is in the form of a nonlinear matrix inequality and the gain matrices $\mathcal{M}_j$ and $\mathcal{N}_j$ are yet to be determined. The necessary condition for stability has been summarized in this theorem and can be used to find the control gains $\mathcal{M}_j$ and $\mathcal{N}_j$ that would stabilize the system.*

3.2. Stabilization analysis

This section provides the RSE and stabilization analysis of PMVG-based WECS (2.12).

Theorem 2. *For known scalars $h_k \in (0, h]$, $\alpha > 0, \gamma > 0, \beta > 0$, and matrices $\varpi > 0$, the constant time-delay $\sigma > 0$, and the RSE of PMVG-based WECS* (2.12) *is bounded in $\epsilon(\varpi, 1)$, if there exists positive symmetric matrices $\bar{\mathcal{Z}}, \bar{Z}_1, \bar{\mathcal{X}}_{11}, \bar{\mathcal{X}}_{14}, \bar{\mathcal{X}}_{16}, \bar{\mathcal{P}}_1, \bar{\mathcal{P}}_3, \bar{T}_1, \bar{Z}_2$, any matrices $\bar{\mathcal{X}}_{12}, \bar{\mathcal{X}}_{13}, \bar{\mathcal{X}}_{15}, \bar{\mathcal{P}}_2, \mathcal{G}, \bar{W}_{1l}, \bar{W}_{2l}$ ($l = 1, 2, 3, 4, 5, 6, 7$), satisfying the following LMIs:*

$$\begin{bmatrix} -\bar{\mathcal{Z}} & \mathcal{G}^T \\ * & -\varpi^{-1} \end{bmatrix} \leq 0, \tag{3.13}$$

$$\begin{bmatrix} \bar{\Theta}^{ij}_{(h_k,0)} & \bar{\Xi}_1 & \frac{h^2}{4}\bar{\Xi}_2 \\ * & -\varepsilon I_n & 0 \\ * & * & -\frac{h^2}{4}\bar{O} \end{bmatrix} < 0, \tag{3.14}$$

$$\begin{bmatrix} \bar{\Theta}^{ij}_{(h_k,h_k)} + h\bar{\Xi}_3 & \bar{W}_{1l} & \bar{W}_{2l} & \bar{\Xi}_1 & \frac{h^2}{4}\bar{\Xi}_2 \\ * & -h\bar{\mathcal{P}}_1 & 0 & 0 & 0 \\ * & * & -\frac{h^3}{3}\bar{\mathcal{P}}_1 & 0 & 0 \\ * & * & * & -\varepsilon I_n & 0 \\ * & * & * & * & -\frac{h^2}{4}\bar{O} \end{bmatrix} < 0, \tag{3.15}$$

$$\begin{aligned}
\bar{\Theta}^{ij}_{(h_k,h(t))} &= Sym\{\mathrm{e}_1^T\bar{\mathcal{Z}}\mathrm{e}_5 + \frac{\pi^2}{4}e^{-\alpha\sigma}\mathrm{e}_3\bar{\mathcal{Z}}_2\mathrm{e}_4 - h(t)(\mathrm{e}_1^T\bar{\mathcal{X}}_{12}\mathrm{e}_2 + \mathrm{e}_1^T\bar{\mathcal{X}}_{13}\mathrm{e}_3 + \mathrm{e}_2^T\bar{\mathcal{X}}_{15}\mathrm{e}_3) \\
&+ (h_k - h(t))(\mathrm{e}_1^T\bar{\mathcal{Z}}_1\mathrm{e}_5 - \mathrm{e}_2^T\bar{\mathcal{Z}}_1\mathrm{e}_5 + \alpha\mathrm{e}_1^T\bar{\mathcal{Z}}_1\mathrm{e}_2 + \mathrm{e}_1^T\bar{\mathcal{X}}_{12}\mathrm{e}_2 + \mathrm{e}_1^T\bar{\mathcal{X}}_{13}\mathrm{e}_3 + \mathrm{e}_2^T\bar{\mathcal{X}}_{15}\mathrm{e}_3 + \mathrm{e}_2^T\bar{\mathcal{P}}_2^T\mathrm{e}_5)\} \\
&+ \bar{\Xi}_4 + \alpha\mathrm{e}_1^T\bar{\mathcal{Z}}\mathrm{e}_1 + \alpha\mathrm{e}_1^T\bar{\mathcal{Z}}_1\mathrm{e}_1 + \alpha\mathrm{e}_1^T\bar{\mathcal{Z}}_1\mathrm{e}_2 - h(t)(\mathrm{e}_1^T\bar{\mathcal{X}}_{11}\mathrm{e}_1 + \mathrm{e}_2^T e^{\alpha h}h(t)\bar{\mathcal{P}}_3\mathrm{e}_2 + \mathrm{e}_2^T\bar{\mathcal{X}}_{14}\mathrm{e}_2 \\
&+ \mathrm{e}_3^T\bar{\mathcal{X}}_{16}\mathrm{e}_3) + (h_k - h(t))(\alpha\mathrm{e}_1^T\bar{\mathcal{Z}}_1\mathrm{e}_1 - \alpha\mathrm{e}_2^T\bar{\mathcal{Z}}_1\mathrm{e}_2 + \mathrm{e}_1^T\bar{\mathcal{X}}_{11}\mathrm{e}_1 + \mathrm{e}_2^T\bar{\mathcal{X}}_{14}\mathrm{e}_2 + \mathrm{e}_3^T\bar{\mathcal{X}}_{16}\mathrm{e}_3 + \mathrm{e}_5^T\bar{\mathcal{P}}_1\mathrm{e}_5 \\
&- \mathrm{e}_2^T\bar{\mathcal{P}}_3\mathrm{e}_2) + \mathrm{e}_5^T\frac{h^2}{4}\bar{O}\mathrm{e}_5 - \mathrm{e}_1^T e^{\alpha h}\bar{\mathcal{P}}_2\mathrm{e}_2 + \mathrm{e}_1^T\sigma\bar{\mathcal{T}}_1\mathrm{e}_1 + \mathrm{e}_2^T 2e^{\alpha h}\bar{\mathcal{P}}_2\mathrm{e}_2 - \mathrm{e}_4^T\sigma e^{-\alpha\sigma}\bar{\mathcal{T}}_1\mathrm{e}_4 + \mathrm{e}_5\bar{\mathcal{Z}}_2\mathrm{e}_5 \\
&- \frac{\pi^2}{4}e^{-\alpha\sigma}(\mathrm{e}_3\bar{\mathcal{Z}}_2\mathrm{e}_3 + \mathrm{e}_4\bar{\mathcal{Z}}_2\mathrm{e}_4) + Sym\{\mathrm{e}_1^T\gamma + \mathrm{e}_3^T + \mathrm{e}_5^T\beta\}[-\bar{\mathcal{G}}\mathrm{e}_5 + \mathcal{A}_i\bar{\mathcal{G}}\mathrm{e}_1 + B_i\mathcal{K}_j\mathrm{e}_2 + B_i\mathcal{L}_j\mathrm{e}_3 \\
&+ D_i\mathrm{e}_7] + \varepsilon\Xi_5 B_i Q_j Q_j^T B_i^T\Xi_5^T,
\end{aligned}$$

$$\bar{\Xi}_1 = (S_j\mathrm{e}_2^T + T_j\mathrm{e}_3^T)diag\{\mathcal{G}\ \mathcal{G}\ \mathcal{G}\ \mathcal{G}\ \mathcal{G}\ \mathcal{G}\ \mathcal{G}\}, \bar{\Xi}_2 = [\bar{\mathcal{X}}_{11}\ \bar{\mathcal{X}}_{12}\ \bar{\mathcal{X}}_{13}\ 0\ 0\ 0\ 0]^T,$$

$$\bar{\Xi}_3 = Sym\{[\bar{W}_{2l}\ \bar{W}_{2l}\ 0\ 0\ 0\ 0\ 0]\}, \bar{\Xi}_4 = Sym\{[\bar{W}_{1l}\ -\bar{W}_{1l}\ 0\ 0\ 0\ 2\bar{W}_{2l}\ 0]\},$$

$$\bar{\Xi}_5 = \mathfrak{e}_1\gamma + \mathfrak{e}_3 + \mathfrak{e}_5\beta,\ \bar{\mathcal{X}} = \begin{bmatrix} \bar{\mathcal{X}}_{11} & \bar{\mathcal{X}}_{12} & \bar{\mathcal{X}}_{13} \\ * & \bar{\mathcal{X}}_{14} & \bar{\mathcal{X}}_{15} \\ * & * & \bar{\mathcal{X}}_{16} \end{bmatrix}, \bar{\mathcal{P}} = \begin{bmatrix} \bar{\mathcal{P}}_1 & \bar{\mathcal{P}}_2 \\ * & \bar{\mathcal{P}}_3 \end{bmatrix}.$$

Moreover, the control gain matrices are calculated by $\mathcal{M}_j = \mathcal{K}_j\mathcal{G}^{-1}$ *and* $\mathcal{N}_j = \mathcal{L}_j\mathcal{G}^{-1}$.

Proof. *Let* $\bar{\mathcal{G}}_1 = \gamma\mathcal{G}^{-1}$, $\bar{\mathcal{G}}_2 = \mathcal{G}^{-1}$, $\bar{\mathcal{G}}_3 = \beta\mathcal{G}^{-1}$, $\mathcal{G}^T\mathcal{Z}\mathcal{G} = \bar{\mathcal{Z}}$, $\mathcal{G}^T\mathcal{Z}_1\mathcal{G} = \bar{\mathcal{Z}}_1$, $\mathcal{G}^T\mathcal{T}_1\mathcal{G} = \bar{\mathcal{T}}_1$, $\bar{\mathcal{X}} = diag(\mathcal{G}^T, \mathcal{G}^T, \mathcal{G}^T)\ \mathcal{X} diag(\mathcal{G}, \mathcal{G}, \mathcal{G})$, $\mathcal{G}^T\mathcal{Z}_2\mathcal{G} = \bar{\mathcal{Z}}_2$, $\bar{\mathcal{P}} = diag(\mathcal{G}^T, \mathcal{G}^T)\mathcal{P} diag(\mathcal{G}, \mathcal{G})$, $\mathcal{G}^T W_{1l}\mathcal{G} = \bar{W}_{1l}$, $\mathcal{G}^T W_{2l}\mathcal{G} = \bar{W}_{2l}$, $\mathcal{K}_j = \mathcal{M}_j\mathcal{G}$, *and* $\mathcal{L}_j = \mathcal{N}_j\mathcal{G}$. *Then, the inequalities* (3.2) *and* (3.3) *are pre-multiplied and post-multiplied by diag* $\{\mathcal{G}^T, \mathcal{G}^T, \mathcal{G}^T, \mathcal{G}^T, \mathcal{G}^T, \mathcal{G}^T, \mathcal{G}^T\}$ *and its transpose, respectively, we obtain LMIs* (3.14) *and* (3.15). *In addition, the overall procedure to verify the feasibility of the PMVG-based WECS* (2.12) *and to obtain the controller gain matrices from Theorem 2 is summarized in Algorithm 1. Hence, this completes the proof.* □

Algorithm 1 Stabilization analysis procedure for PMVG-based WECS

- **Input:** System matrices $\mathcal{A}$, B_i; symmetric matrices $\mathcal{Z}$, $\mathcal{X}$, $\mathcal{P}$, $\mathcal{Z}_1$, $\mathcal{T}_1$, $\mathcal{Z}_2$; positive definite matrix $\mathcal{G}$; sampling interval bound $h_k \in (0, h]$.
- **Output:** Controller gain matrices $\mathcal{M}_j$, $\mathcal{N}_j$ and admissible sampling interval upper bound h.
- **Step 1:** Select positive scalars α, γ, β, $\bar{w}$ and memory parameter $\sigma > 0$.
- **Step 2:** Specify an initial value for sampling upper bound h, and incrementally increase it within an acceptable range.
- **Step 3:** For each trial value of h, check the feasibility of the LMIs given in (3.14) and (3.15).
- **Step 4:** If the LMIs are feasible:
  - Calculate controller gains $\mathcal{M}_j$, $\mathcal{N}_j$ for all j.
  - Store the current value of h as the admissible sampling interval.
  - Terminate.
- **Step 5:** If the LMIs are infeasible:
  - Decrease h and repeat Steps 2–4 until feasibility is achieved.
  - Fine-tune parameters α, γ, β, $\bar{w}$, σ to improve feasibility if needed.

Remark 3. *In Theorems 1 and 2, we provided the asymptotic stability of RSE analysis for the PMVG-based WECS* (2.12). *To illustrate the less-conservative results of the suggested method. In this part, we consider without RSE and disturbance matrices. Then, we have the following two-rule TSFS*

$$\dot{x}(t) = \sum_{i=1}^{2} \varphi_i(\upsilon(t))\{\mathcal{A}_i x(t) + B_i u(t)\}. \tag{3.16}$$

Substituting (2.11) *into* (3.16), *one is able to derive the closed-loop TSFS below*

$$\dot{x}(t) = \sum_{i=1}^{2}\sum_{j=1}^{2} \varphi_i(\upsilon(t))\varphi_j(\upsilon(t_k))\{\mathcal{A}_i x(t) + B_i\{(\mathcal{M}_j + \Delta\mathcal{M}_j(t))x(t - h(t))$$

$$+ (\mathcal{N}_j + \Delta\mathcal{N}_j(t))x(t - h(t) - \sigma)\}. \tag{3.17}$$

Without the use of an exponential term, the appropriate LKF (3.4)–(3.9) *and its derivative can be obtained directly from Theorem 1. After that, the following Corollary can be used to establish the stability condition of system* (3.17).

Corollary 1. *For known scalars $h_k \in (0, h]$, $\gamma > 0$, $\beta > 0$, the constant time-delay $\sigma > 0$, and the gain matrices $\mathcal{M}_j$ and $\mathcal{N}_j$, the TSFS* (3.17) *is asymptotically stable, if there exists positive symmetric matrices $\mathcal{Z}$, $\mathcal{Z}_1$, $\mathcal{X}_{11}$, $\mathcal{X}_{14}$, $\mathcal{X}_{16}$, $\mathcal{P}_1$, $\mathcal{P}_3$, T_1, Z_2, any matrices $\mathcal{X}_{12}$, $\mathcal{X}_{13}$, $\mathcal{X}_{15}$, $\mathcal{P}_2$, $\bar{\mathcal{G}}_1$, $\bar{\mathcal{G}}_2$, $\bar{\mathcal{G}}_3$, W_{1l}, W_{2l} ($l = 1, 2, 3, 4, 5, 6$), satisfying the following LMIs:*

$$\begin{bmatrix} \Pi^{ij}_{(h_k,0)} & \Xi_1 & \frac{h^2}{4}\Xi_2 \\ * & -\varepsilon I_n & 0 \\ * & * & -\frac{h^2}{4}\mathcal{O} \end{bmatrix} < 0, \tag{3.18}$$

$$\begin{bmatrix} \Pi^{ij}_{(h_k,hk)} + h\Xi_3 & W_{1l} & W_{2l} & \Xi_1 & \frac{h^2}{4}\Xi_2 \\ * & -h\mathcal{P}_1 & 0 & 0 & 0 \\ * & * & -\frac{h^3}{3}\mathcal{P}_1 & 0 & 0 \\ * & * & * & -\varepsilon I_n & 0 \\ * & * & * & * & -\frac{h^2}{4}\mathcal{O} \end{bmatrix} < 0, \tag{3.19}$$

where $\Pi^{ij}_{(h_k,h(t))}$ can be stated as

$$\begin{aligned}
\Pi^{ij}_{(h_k,h(t))} &= Sym\{\mathrm{e}_1^T\mathcal{Z}\mathrm{e}_5 + \frac{\pi^2}{4}\mathrm{e}_3\mathcal{Z}_2\mathrm{e}_4 - h(t)(\mathrm{e}_1^T\mathcal{X}_{12}\mathrm{e}_2 + \mathrm{e}_1^T\mathcal{X}_{13}\mathrm{e}_3 + \mathrm{e}_2^T\mathcal{X}_{15}\mathrm{e}_3)(h_k - h(t)) \\
&\times (\mathrm{e}_1^T\mathcal{Z}_1\mathrm{e}_5 - \mathrm{e}_2^T\mathcal{Z}_1\mathrm{e}_5 + \mathrm{e}_1^T\mathcal{X}_{12}\mathrm{e}_2 + \mathrm{e}_1^T\mathcal{X}_{13}\mathrm{e}_3 + \mathrm{e}_2^T\mathcal{X}_{15}\mathrm{e}_3 + \mathrm{e}_2^T\mathcal{P}_2^T\mathrm{e}_5)\} + \Xi_4 - h(t)(\mathrm{e}_1^T\mathcal{X}_{11}\mathrm{e}_1 \\
&+ \mathrm{e}_2^T h(t)\mathcal{P}_3\mathrm{e}_2 + \mathrm{e}_2^T\mathcal{X}_{14}\mathrm{e}_2 + \mathrm{e}_3^T\mathcal{X}_{16}\mathrm{e}_3) + (h_k - h(t))(\mathrm{e}_1^T\mathcal{X}_{11}\mathrm{e}_1 + \mathrm{e}_2^T\mathcal{X}_{14}\mathrm{e}_2 + \mathrm{e}_3^T\mathcal{X}_{16}\mathrm{e}_3 \\
&+ \mathrm{e}_5^T\mathcal{P}_1\mathrm{e}_5 - \mathrm{e}_2^T\mathcal{P}_3\mathrm{e}_2) + \mathrm{e}_5^T\frac{h^2}{4}\mathcal{O}\mathrm{e}_5 - \mathrm{e}_1^T\mathcal{P}_2\mathrm{e}_2 + \mathrm{e}_2^T 2\mathcal{P}_2\mathrm{e}_2 + \mathrm{e}_1^T\sigma\mathcal{T}_1\mathrm{e}_1 - \mathrm{e}_4^T\sigma\mathcal{T}_1\mathrm{e}_4 + \mathrm{e}_5\mathcal{Z}_2\mathrm{e}_5 \\
&- \frac{\pi^2}{4}(\mathrm{e}_3\mathcal{Z}_2\mathrm{e}_3 + \mathrm{e}_4\mathcal{Z}_2\mathrm{e}_4) + Sym\{\mathrm{e}_1^T\bar{\mathcal{G}}_1^T + \mathrm{e}_3^T\bar{\mathcal{G}}_2^T + \mathrm{e}_5^T\bar{\mathcal{G}}_3^T\}[-\mathrm{e}_5 + \mathcal{A}_i\mathrm{e}_1 + B_i\mathcal{M}_j\mathrm{e}_2 \\
&+ B_i\mathcal{N}_j\mathrm{e}_3 + D_i\mathrm{e}_7] + \varepsilon\Xi_5 B_i Q_j Q_j^T B_i^T\Xi_5^T, \\
\Xi_1 &= (S_j\mathrm{e}_2^T + T_j\mathrm{e}_3^T)diag\{\mathcal{G}\,\mathcal{G}\,\mathcal{G}\,\mathcal{G}\,\mathcal{G}\,\mathcal{G}\,\mathcal{G}\}, \ \Xi_2 = [\mathcal{X}_{11}\ \mathcal{X}_{12}\ \mathcal{X}_{13}\ 0\ 0\ 0]^T, \\
\Xi_3 &= Sym\{[W_{2l}\ W_{2l}\ 0\ 0\ 0\ 0]\}, \Xi_4 = Sym\{[W_{1l}\ -W_{1l}\ 0\ 0\ 0\ 2W_{2l}]\}, \\
\Xi_5 &= \mathrm{e}_1 M_1^T + \mathrm{e}_3 M_2^T + \mathrm{e}_5 M_3^T, \\
\mathcal{X} &= \begin{bmatrix} \mathcal{X}_{11} & \mathcal{X}_{12} & \mathcal{X}_{13} \\ * & \mathcal{X}_{14} & \mathcal{X}_{15} \\ * & * & \mathcal{X}_{16} \end{bmatrix}, \ \mathcal{P} = \begin{bmatrix} \mathcal{P}_1 & \mathcal{P}_2 \\ * & \mathcal{P}_3 \end{bmatrix}.
\end{aligned}$$

Proof. Similar to Theorem 1, the proof can be obtained straightforwardly. □

4. Numerical simulation

This section demonstrates the applicability and effectiveness of the theoretical findings through comprehensive numerical validation. The performance of the proposed NFMSDC scheme is

evaluated through two distinct case studies within Example 1, each addressing critical operational scenarios in PMVG-based WECS. Although the proposed controller design requires solving LMIs, these computations are performed offline during the controller design stage. Once the controller gains are obtained, the online implementation requires only simple matrix multiplications, which are computationally efficient for real-time control platforms. Additionally, Example 2 provides comparative analysis demonstrating the superiority of the proposed approach over existing methods.

Example 1. *Application to PMVG-based WECS* (2.12) *under different operational scenarios*

This example comprehensively evaluates the RSE and stabilization performance of the considered system (2.12) under the proposed NFMSDC scheme through two critical case studies that reflect realistic operating conditions of wind energy systems. The simulation parameters of the PMVG-based WECS are presented in Table 1. Then, we selected $Q = [0.01\ 0.01\ 0.01]$, $S = 0.01I_3$, $T = 0.01I_3$, $R = 0.1sin(t)I_3$ to ensure appropriate weighting in the control design. Based on the stabilization conditions for PMVG-based WECS (2.12) in Theorem 2, we take the scalars $\alpha = 10.1, \gamma = 5.01, \beta = 10.02$, $\bar{w} = 10.001$, $\theta_{max} = 0.003$ and constant time-delay $\sigma = 0.2$, and obtained the MSI $h = 0.01$. Applying Theorem 2 with the aforementioned parameters, the following control gain matrices are obtained:

$$\mathcal{M}_1 = \begin{bmatrix} -111.8467 & -987.1744 & 30.8889 \\ -12.8611 & -72.3171 & -674.4295 \end{bmatrix},$$
$$\mathcal{M}_2 = \mathcal{M}_3 = \mathcal{M}_4 = \mathcal{M}_1.$$
$$\mathcal{N}_1 = \begin{bmatrix} -0.0441 & -0.8211 & -0.0753 \\ -0.1064 & 0.0316 & -0.4899 \end{bmatrix},$$
$$\mathcal{N}_2 = \mathcal{N}_3 = \mathcal{N}_4 = \mathcal{N}_1.$$

Table 1. Simulation parameters of PMVG-based WECS [4].

Parameters	Symbol	Value
Rated power	$P_{turbine}$	5-kW
Maximum power coefficient	C_{pmax}	0.441
Tip speed ratio	λ	8.1
air density	ρ	1.225 kg/m^3
Modulation flux linkage	Ψ_{mag}	0.01
Winding resistance of stator	R_s	1 Ω
$d-q$ frame inductance	$L_d = L_q$	17.5 mH
Modulation flux linkage	Ψ_{mag}	0.4459 rad/s
Pole pairs	n_p	0.001
Total moment of inertia	J	0.18 $kg.m^2$
Viscous friction	f_c	$0.4924e^{-}3$ $N.m.s$

Case 1: Wind-induced disturbance analysis. This case study examines the system behavior under realistic wind disturbance conditions, which represent the primary external perturbation in wind energy systems. The wind-induced disturbance is modeled as described in Eq (2.8), capturing the stochastic accumulated nature of wind variability. Figure 3(a) visually presents the disturbance profile

$w(t)$ as described in Eq (2.8). The plot illustrates the stochastic nature of the disturbance, capturing the accumulated temporal fluctuations resulting from the integrated Gaussian noise process. This disturbance input, characterized by continuous random variations, represents realistic wind variability imposed on the system. The figure provides insight into the intensity and dynamic variation of the wind disturbance over the simulation period, which poses a challenging environment for controller performance evaluation.

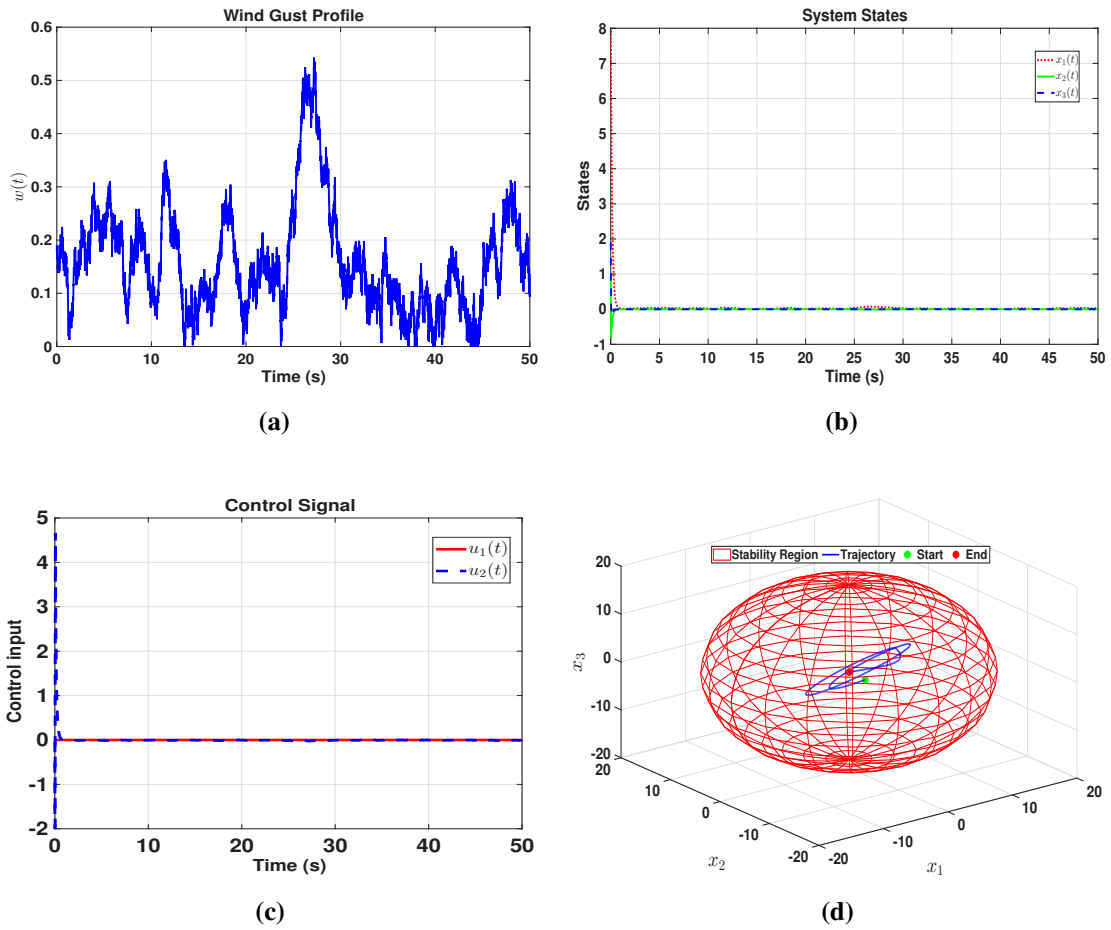

Figure 3. Performance evaluation of the proposed method for PMVG-based WECS under wind disturbances: (a) wind disturbance, (b) system states, (c) control input, (d) RSE boundaries and state trajectories.

In addition, the state trajectories of PMVG-based WECS (2.12) are displayed in Figure 3(b). The results demonstrate effective stabilization with all state trajectories converging smoothly toward the equilibrium points without excessive oscillations or divergence. This behavior confirms the ability of the NFMSDC to robustly regulate key electrical variables despite the persistent wind disturbances, maintaining operational stability and ensuring safety margins are respected. Figure 3(c) illustrates the control trajectory of the designed NFMSDC scheme. This effective control effort highlights the broad applicability of the proposed scheme in compensating for wind disturbances while preserving smooth control action. The RSE bound represents a mathematically derived ellipsoidal region which quantifies

the guaranteed stability domain for the system states under the combined effect of control uncertainties and external disturbances. Figure 3(d) displays the state trajectories of the system alongside the boundary ellipsoid. From Figure 3(d), one can confirm that the RSE for the PMVG-based WECS is bounded by the derived ellipsoid $\epsilon(\varpi, 1)$ under the NFMSDC technique. This containment of trajectories within the ellipsoid validates the robustness and efficacy of the control design, ensuring the system stability and safe operation under disturbance case. From a practical perspective, the reachable set estimation represents a safety region within which the system states are guaranteed to remain under bounded disturbances and controller uncertainties. The ellipsoidal bound obtained from the proposed approach provides an explicit characterization of this safe operating region for the PMVG-based WECS.

Case 2: Parameter variation analysis. This case study assesses the robustness of the NFMSDC scheme against practical parameter uncertainties in the PMVG-based WECS. The examined parameters include L_d, L_q, Ψ_{mag}, J, and R_s, which are subject to variations due to temperature effects, magnetic saturation, and contact resistance. The parameter variations are applied systematically in increments defined by:

1. -10% variation: Parameters decreased by 10% from the nominal values.
2. Nominal values: Baseline parameters without modification.
3. $+10\%$ variation: Parameters increased by 10% over nominal values.

The simulation results, as shown in Figure 4, demonstrate that the proposed NFMSDC scheme maintains stable system responses under different parameter uncertainty levels. Even when multiple parameters vary simultaneously within the considered range (-10%, nominal, and $+10\%$), the system states converge smoothly to the equilibrium point without instability or excessive oscillations. These results confirm the robustness of the proposed controller against modeling uncertainties that commonly occur in practical wind energy systems.

The corresponding control inputs, displayed in Figure 5, demonstrate the effectiveness of the proposed non-fragile memory sampled-data control. The control signals remain within practical actuator limits without requiring manual retuning or gain scheduling. The controller adapts smoothly under varying parameter conditions, ensuring stable state trajectories while preserving overall control efficiency.

The corresponding RSE bounds, displayed in Figure 6, illustrate the robustness of the proposed NFMSDC against parameter variations. The estimated bounds remain compact and stable, confirming that the controller successfully limits state deviations within predictable regions. Even under parameter fluctuations, the RSE demonstrates that the closed-loop system preserves safety and stability without additional tuning of the controller.

The disturbance model and the simulation results in Figures 3–6 shows that the proposed NFMSDC controller is effective for stabilizing the PMVG-based WECS under wind changes and parameter variations. The results confirm that the proposed controller keeps the system stable, guides the states smoothly, and uses the control input efficiently. It also works without frequent maintenance or recalibration, keeping steady performance over time. This strong ability to handle disturbances and parameter changes helps lower operating costs, improve system reliability, and give more flexibility for wind energy systems in different conditions.

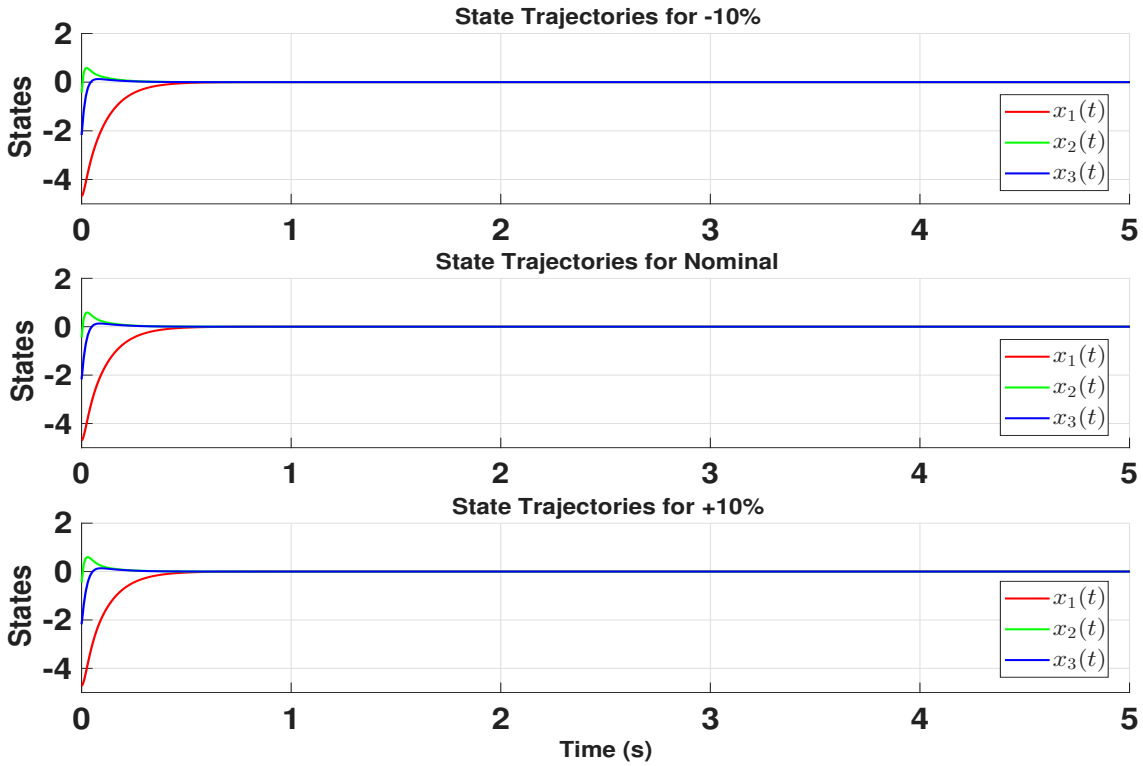

Figure 4. State response of PMVG-based WECS (2.12) under the proposed NFMSDC for each parameter variation.

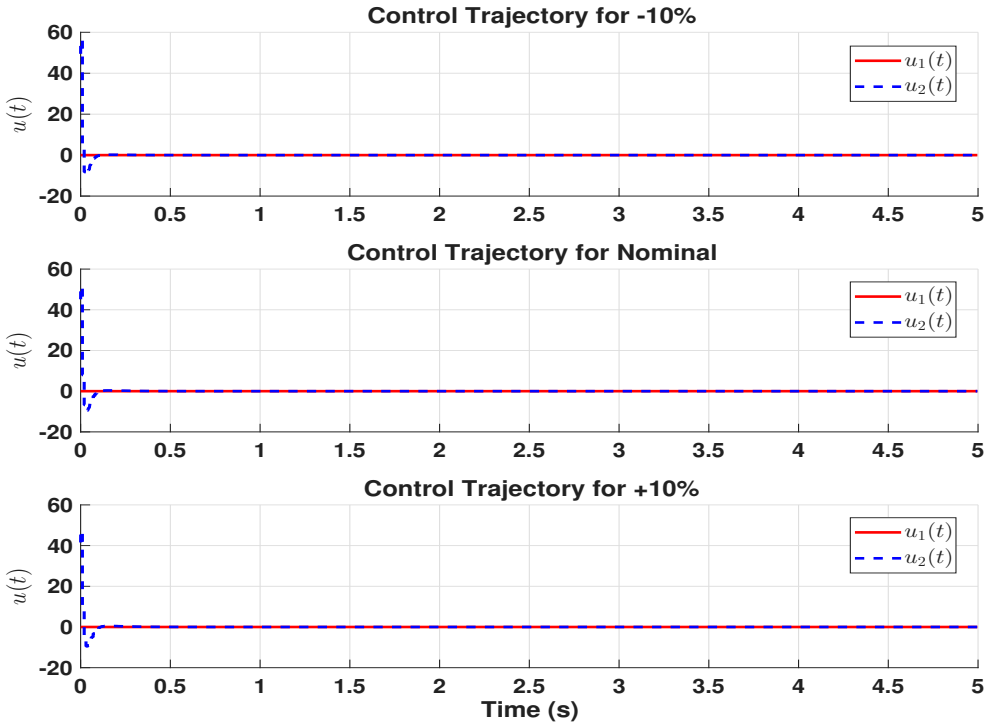

Figure 5. Response of proposed NFMSDC (2.11) trajectories under parameter variation.

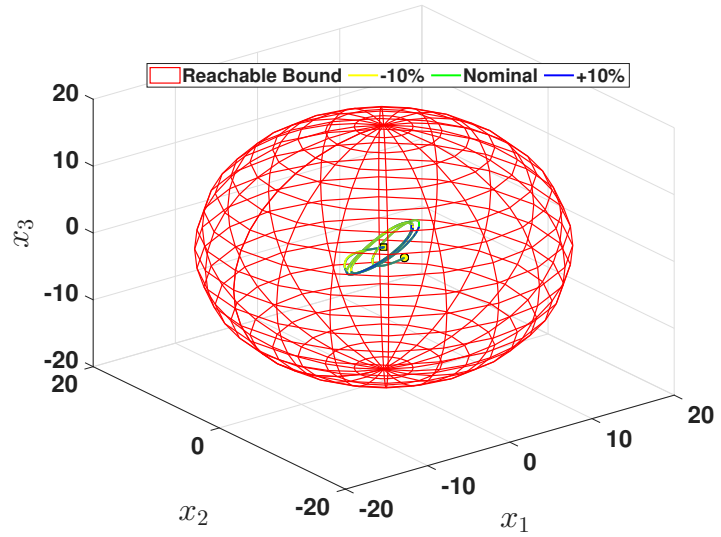

Figure 6. RSE boundaries and state trajectories of PMVG-based WECS (2.12) in Theorem 2 under parameter variations.

Example 2. *Comparative result analysis*

To further validate the proposed method, consider the PMSM system in [23] described by the ODE dynamics in (4.1). The numerical validation uses the system parameters provided in Table II of [23], with the following dynamics can be taken into consideration.

$$\begin{cases} \dot{x}_1(t) &= -x_1(t) + x_2(t)x_3(t) + u(t) \\ \dot{x}_2(t) &= -x_2(t) + x_3(t)(\gamma\gamma - x_1(t)) + u(t) \\ \dot{x}_3(t) &= v(x_2(t) - x_3(t)) \end{cases} \tag{4.1}$$

where $x_1(t)$, $x_2(t)$, and $x_3(t)$ denote the state variables of the system (4.1). $u(t)$ is the control vector. $\gamma\gamma$ and v represent the known constant variables. By applying the proposed NFMSDC and following the system in Corollary 3 without RSE and disturbance terms, the closed-loop system can be expressed as a delay differential system:

$$\dot{x}(t) = \sum_{i=1}^{2}\sum_{j=1}^{2} \varphi_i(x_3(t))\varphi_j(x_3(t_k))\{\mathcal{A}_i x(t) + B_i\{(\mathcal{M}_j + \Delta\mathcal{M}_j(t))x(t - h(t)) + (\mathcal{N}_j + \Delta\mathcal{N}_j(t))x(t - h(t) - \sigma)\}. \tag{4.2}$$

Then, the PMSM system dynamics can be expressed by the following matrices:

$$A_1 = \begin{bmatrix} -1 & d_1 & 0 \\ -d_1 & -1 & \gamma\gamma \\ 0 & v & -v \end{bmatrix}, A_2 = \begin{bmatrix} -1 & -d_1 & 0 \\ d_1 & -1 & \gamma\gamma \\ 0 & v & -v \end{bmatrix}, B_1 = B_2 = \begin{bmatrix} 1 \\ 1 \\ 0 \end{bmatrix}.$$

Following this, the membership functions are

$$h_1(x_3(t)) = \frac{1}{2}\left(1 + \frac{x_3(t)}{d_1}\right), \; h_2(x_3(t) = 1 - h_1(x_3(t))).$$

Consider $d_1 = 12, \gamma\gamma = 1.1$, and $v = 5.46$. The positive scalars $\gamma = 2.1, \beta = 20$ and the constant delay $\sigma = 0.01$. Then, we selected $Q = [0.02\ 0.01\ 0.01]$, $S = 0.001I_3$, $T = 0.001I_3$, $R = cos(t)I_3$. Based on the above LMIs (3.18) and (3.19) in Corollary 1, we can obtain the MSI $h = 0.09$. In this respect, the control gain matrices that correspond are as follows:

$$\mathcal{M}_1 = 10^3 \times \begin{bmatrix} -0.0450 & -0.0475 & 0.0682 \end{bmatrix},\ \mathcal{M}_2 = \mathcal{M}_1.$$
$$\mathcal{N}_1 = \begin{bmatrix} -0.2111 & -0.2211 & 0.0005 \end{bmatrix},\ \mathcal{N}_2 = \mathcal{N}_1.$$

From these results, it is evident that the proposed NFMSDC method achieves a larger maximum allowable sampling interval $h = 0.09$ compared to the existing method in [23], as shown in Table 2. Numerical simulations further confirm the feasibility and effectiveness of the controller design presented in Corollary 1, demonstrating its robustness and superiority in stabilizing the PMSM system described by (4.2).

Table 2. Maximum upper bound.

Methods	Maximum h
[23]	0.06
Corollary 1	0.09

5. Conclusions

In this paper, the problem of reachable set estimation (RSE) and stabilization has been investigated for a real-time 5-kW PMVG-based wind energy conversion system under an NFMSDC framework, considering constant transmission delays and controller gain uncertainties. The proposed approach integrates RSE with SDC design through a looped LKF framework, and delay-dependent stability conditions are derived in terms of linear matrix inequalities. The effectiveness of the proposed method is verified through comprehensive numerical simulations. In Example 1, the controller performance is evaluated through two case studies. Case 1 demonstrates effective disturbance rejection while maintaining the system states within the designed reachable set bounds. Case 2 confirms robust stabilization under simultaneous variations of key system parameters. In Example 2, the proposed method is compared with existing approaches, where the NFMSDC scheme achieves larger admissible sampling intervals, indicating improved delay tolerance and enhanced robustness. Compared with existing studies, the proposed framework provides a unified control strategy that simultaneously addresses RSE, nonlinear system dynamics, sampling constraints, transmission delays, and controller gain perturbations for PMVG-based WECS. These features highlight the theoretical and practical advantages of the proposed approach. Nevertheless, this study assumes constant transmission delays and known uncertainty bounds. Future work will focus on extending the proposed framework to systems with time-varying delays and networked multi-agent wind energy systems. In addition, further investigation will consider practical implementation aspects, including real-time embedded control platforms and field-deployed wind energy applications.

Author contributions

R. Venkateswaran: Conceptualization, methodology, formal analysis, validation, writing – original draft; W. Choi: Method-validation, writing – review and editing; J. H. Jeong: Supervision, method-validation, writing – review and editing; J. Woo: Supervision, method-validation, writing – review and editing. All authors have read and approved the final version of the manuscript for publication.

Use of Generative-AI tools declaration

The authors declare they have not used Artificial Intelligence (AI) tools in the creation of this article.

Conflict of interest

The authors declare that they have no conflict of interest.

References

1. G. Mayilsamy, S. R. Lee, Y. H. Joo, An improved model predictive control of back-to-back three-level NPC converters with virtual space vectors for high power PMSG-based wind energy conversion systems, *ISA T.,* **143** (2023), 503–524. https://doi.org/10.1016/j.isatra.2023.09.033
2. G. Narayanan, M. S. Ali, S. Ahn, Y. H. Joo, R. Karthikeyan, G. Rajchakit, Fractional impulsive controller design of fractional-order fuzzy systems with average dwell-time strategy and its application to wind energy systems, *Commun. Nonlinear Sci.,* **140** (2025), 108394. https://doi.org/10.1016/j.cnsns.2024.108394
3. R. Venkateswaran, S. R. Lee, Y. H. Joo, Stability augmentation of pitch angle control for maximum power extraction of PMSG-based WTS with pitch actuator uncertainty via L1 adaptive scheme, *Int. J. Elec. Power,* **153** (2023), 109392. https://doi.org/10.1016/j.ijepes.2023.109392
4. K. Palanimuthu, G. Mayilsamy, S. R. Lee, S. Y. Jung, Y. H. Joo, Comparative analysis of maximum power extraction and control methods between PMSG and PMVG-based wind turbine systems, *Int. J. Elec. Power,* **143** (2022), 108475. https://doi.org/10.1016/j.ijepes.2022.108475
5. G. Narayanan, J. J. Hoon, J. Y. Hoon, Resilient sampled-data control for fractional-order PMVG-based WTS with actuator saturation and probabilistic faults using fuzzy Lyapunov function method, *Inform. Sci.,* **686** (2025), 121294. https://doi.org/10.1016/j.ins.2025.121294
6. N. Gunasekaran, Y. H. Joo, Robust sampled-data fuzzy control for nonlinear systems and its applications: Free-weight matrix method, *IEEE T. Fuzzy Syst.,* **27** (2019), 2130–2139. https://dx.doi.org/10.1109/TFUZZ.2019.2893566
7. M. S. Aslam, H. Bilal, A. V. Vasilakos, Self-triggered scheme design for Takagi–Sugeno fuzzy model based on mismatch premise variable with time-varying delay, *IEEE T. Autom. Sci. Eng.,* **22** (2025), 15536–15548. https://doi.org/10.1109/TASE.2025.3570089
8. N. Gunasekaran, R. Saravanakumar, M. S. Ali, Q. Zhu, Exponential sampled-data control for T-S fuzzy systems: Application to Chua's circuit, *Int. J. Syst. Sci.,* **50** (2019), 2979–2992. https://doi.org/10.1080/00207721.2019.1691753

9. R. Venkateswaran, Y. H. Joo, Stabilization of DFIG-based wind turbine with active and reactive power: A coupling memory state-feedback control scheme, *Inform. Sci.,* **648** (2023), 119468. https://doi.org/10.1016/j.ins.2023.119468
10. L. Shanmugam, Y. H. Joo, Adaptive neural networks-based integral sliding mode control for T-S fuzzy model of delayed nonlinear systems, *Appl. Math. Comput.,* **450** (2023), 127983. https://doi.org/10.1016/j.amc.2023.127983
11. V. Dhanya, A. Arunkumar, K. Chaisena, Sampled-data based fault-tolerant control design for uncertain CE151 helicopter system with random delays: Takagi–Sugeno fuzzy approach, *Fractal Fract.,* **6** (2022), 498. https://doi.org/10.3390/fractalfract6090498
12. A. Kashkynbayev, R. Rakkiyappan, Sampled-data output tracking control based on T–S fuzzy model for cancer-tumor-immune systems, *Commun. Nonlinear Sci.,* **128** (2024), 107642. https://dx.doi.org/10.1016/j.cnsns.2023.107642
13. A. A. Yesudhas, S. Kuppusamy, S. R. Lee, J. H. Jeong, Y. H. Joo, Switched sampled-data-based membership function-dependent H_∞ control for PMSG-based WTS with actuator failures, *Math. Comput. Simulat.,* **226** (2024), 560–577. https://doi.org/10.1016/j.matcom.2024.07.023
14. H. Zhao, X. Wang, Robust H_∞ control of switched nonlinear systems under sampled data, *J. Syst. Sci. Complex.,* **35** (2022), 1785–1807. https://doi.org/10.1007/s11424-022-1039-2
15. R. Vadivel, Z. T. Njitacke, L. Shanmugam, P. Hammachukiattikul, N. Gunasekaran, Dynamical analysis and reachable set estimation of T–S fuzzy system with permanent magnet synchronous motor, *Commun. Nonlinear Sci.,* **125** (2023), 107407. https://dx.doi.org/10.1016/j.cnsns.2023.107407
16. A. A. Yesudhas, S. R. Lee, J. H. Jeong, Y. H. Joo, Design of fuzzy dissipative sampled-data control for nonlinear wind turbine systems with random packet losses and communication delays, *Eur. Phys. J.-Spec. Top.,* **234** (2025), 1361—1378. https://dx.doi.org/10.1140/epjs/s11734-024-01249-5
17. R. Vadivel, S. Sabarathinam, Y. Wu, K. Chaisena, N. Gunasekaran, New results on T–S fuzzy sampled-data stabilization for switched chaotic systems with its applications, *Chaos Soliton. Fract.,* **164** (2022), 112741. https://dx.doi.org/10.1016/j.chaos.2022.112741
18. N. Gunasekaran, Y. H. Joo, Nie–Tan fuzzy method of fault-tolerant wind energy conversion systems via sampled-data control, *IET Control Theory A.,* **14** (2020), 1516–1523. https://doi.org/10.1049/iet-cta.2019.0816
19. L. Shanmugam, K. Palanimuthu, Y. H. Joo, Decentralized sampled-data control for stochastic disturbance in interconnected power systems with PMSG-based wind turbines, *IEEE T. Cybernetics,* **54** (2024), 3516–3525. https://dx.doi.org/10.1109/TCYB.2023.3302294
20. R. Zhang, D. Zeng, J. H. Park, Y. Liu, S. Zhong, A new approach to stabilization of chaotic systems with nonfragile fuzzy proportional retarded sampled-data control, *IEEE T. Cybernetics,* **49** (2018), 3218–3229. https://dx.doi.org/10.1109/TCYB.2018.2831782
21. R. Venkateswaran, Y. H. Joo, Retarded sampled-data control design for interconnected power system with DFIG-based wind farm: LMI approach, *IEEE T. Cybernetics,* **52** (2022), 5767–5777. https://dx.doi.org/10.1109/TCYB.2020.3042543

22. K. Subramanian, P. Muthukumar, H. Trinh, Nonfragile sampled-data H_∞ control design for high-speed train with parametric uncertainties, *Int. J. Robust Nonlin.,* **31** (2021), 1021–1034. https://doi.org/10.1002/rnc.5330

23. S. Kuppusamy, Y. H. Joo, Nonfragile retarded sampled-data switched control of T–S fuzzy systems and its applications, *IEEE T. Fuzzy Syst.,* **28** (2019), 2523–2532. https://dx.doi.org/10.1109/TFUZZ.2019.2940432

24. Y. Liu, B. Z. Guo, J. H. Park, S. M. Lee, Nonfragile exponential synchronization of delayed complex dynamical networks with memory sampled-data control, *IEEE T. Neur. Net. Lear.,* **29** (2016), 118–128. https://dx.doi.org/10.1109/TNNLS.2016.2614709

25. C. Jiang, J. Xia, J. Wang, H. Shen, H_∞ control for singularly perturbed semi-Markov jump systems under denial of service attacks, *J. Syst. Sci. Complex.,* **38** (2025), 1568–1582. https://doi.org/10.1007/s11424-025-4435-6

26. D. Velmurugan, A. Arumugam, K. Arumugam, Finite-time observer-based fault detection with nonfragile control design for switched nonlinear networked systems with time-delays, *Optim. Contr. Appl. Met.,* **45** (2024), 248–273. https://doi.org/10.1002/oca.3056

27. A. Arunkumar, J. L. Wu, Observer-based non-fragile event-triggered control of extra-corporeal blood circulation process in finite-time interval, *Int. J. Robust Nonlin.,* **34** (2024), 2141–2161. https://doi.org/10.1002/rnc.7074

28. D. Tong, B. Ma, Q. Chen, Y. Wei, P. Shi, Finite-time synchronization and energy consumption prediction for multilayer fractional-order networks, *IEEE T. Circuits-II,* **70** (2023), 2176–2180. https://dx.doi.org/10.1109/TCSII.2022.3233420

29. M. Shi, D. Tong, Q. Chen, W. Zhou, Pth moment exponential synchronization for delayed multi-agent systems with Lévy noise and Markov switching, *IEEE T. Circuits-II,* **71** (2024), 697–701. https://dx.doi.org/10.1109/TCSII.2023.3304635

30. B. Visakamoorthi, K. Subramanian, P. Muthukumar, Hidden Markov model based non-fragile sampled-data control design for mode-dependent fuzzy systems with actuator faults, *Appl. Math. Comput.,* **435** (2022), 127454. https://dx.doi.org/10.1016/j.amc.2022.127454

31. N. Zhao, D. Lun, H. Zhang, X. Zhao, I. J. Rudas, Composite anti-disturbance control for networked systems with disturbances and actuator attacks via event-triggered output feedback, *IEEE T. Cybernetics,* **56** (2026), 393–403. https://doi.org/10.1109/TCYB.2025.3609819

32. Z. Zuo, Z. Wang, Y. Chen, Y. Wang, A non-ellipsoidal reachable set estimation for uncertain neural networks with time-varying delay, *Commun. Nonlinear Sci.,* **19** (2014), 1097–1106. http://dx.doi.org/10.1016/j.cnsns.2013.08.015

33. Z. Zuo, D. W. Ho, Y. Wang, Reachable set bounding for delayed systems with polytopic uncertainties: The maximal Lyapunov–Krasovskii functional approach, *Automatica,* **46** (2010), 949–952. http://dx.doi.org/10.1016/j.automatica.2010.02.022

34. Z. Feng, W. X. Zheng, L. Wu, Reachable set estimation of T–S fuzzy systems with time-varying delay, *IEEE T. Fuzzy Syst.,* **25** (2016), 878–891. https://doi.org/10.1109/TFUZZ.2016.2586945

35. J. Zhao, Z. Hu, Improved results on reachable set estimation of linear systems, *Int. J. Control Autom.,* **17** (2019), 1141–1148. http://dx.doi.org/10.1007/s12555-018-9728-2

36. S. Jin, Y. Pang, X. Zhou, A. Yan, W. Wang, W. Hu, Robust finite-time control and reachable set estimation for uncertain switched neutral systems with time delays and input constraints, *Appl. Math. Comput.,* **407** (2021), 126321. https://dx.doi.org/10.1016/j.amc.2021.126321

37. T. Li, C. Zheng, Z. Feng, T. N. Dinh, T. Raïssi, Real-time reachable set estimation for linear time-delay systems based on zonotopes, *Int. J. Syst. Sci.,* **54** (2023), 1639–1647. https://doi.org/10.1080/00207721.2023.2189534

38. Z. Zhong, R. J. Wai, Z. Shao, M. Xu, Reachable set estimation and decentralized controller design for large-scale nonlinear systems with time-varying delay and input constraint, *IEEE T. Fuzzy Syst.,* **25** (2016), 1629–1643. https://doi.org/10.1109/TFUZZ.2016.2617366

39. B. Visakamoorthi, P. Muthukumar, H. Trinh, Reachable set estimation for T–S fuzzy Markov jump systems with time-varying delays via membership function dependent performance, *IEEE T. Fuzzy Syst.,* **30** (2022), 4980–4990. https://doi.org/10.1109/TFUZZ.2022.3164799

AIMS Press